Check for updates

Hepatotoxicity of graphene oxide in Wistar rats

Naresh K. Nirmal[1] · Kumud K. Awasthi[2] · Placheril J. John[1]

Abstract

Graphene oxide (GO) has a multitude of applications in areas of nanomedicine, electronics, textile, water purification, and catalysis among others. GO is relatively easier to manufacture and customize as compared with other carbon-based nanomaterials. In the present work, GO was administered intraperitoneally to adult Wistar rats in four incremental doses, i.e., 0.0 mg/kg (control), 0.4 mg/kg (low dose), 2.0 mg/kg (mid-dose), and 10.0 mg/kg (high dose). After 15 repeated doses over a period of 30 days, biochemical assays for alanine transaminase (ALT), aspartate transaminase (AST), alkaline phosphatase (ALP), catalase (CAT), and malondialdehyde (MDA) were carried out. Histopathological and morphometric analyses of liver and kidney were also performed. Results demonstrated dose-dependent toxicity of GO. General behavior and liver indices remained unaffected in the study. Serum levels of ALT, ALP, and AST were altered significantly in high-dose treated animals. Changes were found insignificant in the low- and mid-dose groups. Catalase activity in liver tissue homogenates was decreased in the high-dose group. MDA levels were found elevated in treated rats. Unlike control and low dose, mid- and high-dose treated rats exhibited varying degrees of histopathological changes like inflammation around the central vein and portal veins, vacuolations, hepatocytic injury, and near normal to abnormal hepatic sinusoids. These findings show that GO has considerable toxic potential to mammalian liver and thorough toxicity studies are needed before these nanosheets are used in biomedicine.

Keywords Nanosheets · Graphene oxide · Hepatotoxicity · Nanotoxicity · Toxicity · Liver

Introduction

Graphene oxide (GO) has emerged as an important nanomaterial with its unique physico-chemical attributes in recent years. It has two-dimensional hexagonal lattice structure with epoxy, hydroxy, and other oxygen-containing functional groups (Dreyer et al. 2010). This type of structure increases its solubility in aqueous medium. Unlike pristine graphene sheets, due to the presence of multiple functional groups, it has a great functionalization potential making it suitable for biomedical

✉ Placheril J. John
  placheriljohn@gmail.com

[1] Department of Zoology, University of Rajasthan, Jaipur 302004, India

[2] Department of Life Sciences, Vivekananda Global University, Jaipur 303012, India

applications (Saha et al. 2010). Its potential applications have been demonstrated in biomedicine (Shen et al. 2012; Pang et al. 2017; Wang et al. 2017; Priyadarsini et al. 2018), nanocomposites (Khan et al. 2015; Phiri et al. 2017; Mohan et al. 2018), catalysis (Lonkar and Abdala 2014), biosensors (Beitollahi et al. 2019), and electronics (Singh and Tripathi 2018; Das et al. 2018; Yang et al. 2019) among others. Some recent reviews have comprehensively dealt with potential applications of graphene oxide (Ou et al. 2016; Coros et al. 2019).

Biomedical applications of GO are immense and therefore, thorough scrutiny of its biocompatibility and toxicity is imperative. Many studies have demonstrated toxic effects due to the exposure of GO. At an intravenous dose of 0.4 mg/mouse, GO induced long-term toxicity and impacted major organs, namely liver, spleen, kidney, and lung (Wang et al. 2011). Li et al. (2013) demonstrated that graphene oxide nanosheets bearing sharp edges penetrated into cells and resulted into systemic toxic effects. Li et al. (2016) also found that GO at a dose of 10 mg/kg caused inflammation of the lung, liver, and spleen after a sub-acute exposure. Patlolla et al. (2017) provided evidence of a dose-dependent toxicity to hepatic tissue in rats. The group found increased levels of lipid peroxidation in the tissue and histopathological alterations in rats treated

with 20 and 40 mg/kg doses of GO. However, short-term inhalation exposure to male Sprague-Dawley rats did not produce noticeable toxicity in lungs and other organs even at moderate and high concentrations (Kim et al. 2018). Similarly, Mendonça et al. (2016) reported that reduced GO at a dose of 7 mg/kg had insignificant toxic effects. These contrasting reports present a challenge for nanotoxicity assessments. Further studies are, therefore, required to ascertain biocompatibility of GO. The present study is an effort in this direction to explore impacts of GO exposure in Wistar rat model over a sub-acute exposure schedule.
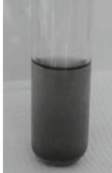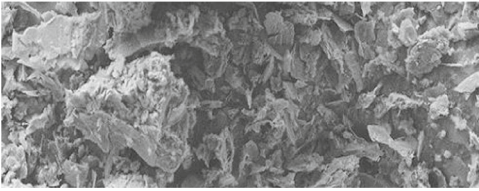
Materials and methods

Graphene oxide

The GO powder was commercially procured from InventyS Research Company Pvt. Ltd., Mumbai (India), and re-characterized to confirm its attributes. Sheet thickness was 0.8–2 nm and average lateral dimensions were 5–10 μm (Table 1). Characterization details shown in the table have already been published (Nirmal et al. 2017b). Additional characterization data of GO is available in the Online Resource. FTIR data confirmed the presence of various functional groups like COOH, CO, and OH (ESM_2).

Animal handling and GO administration

Healthy adult male Wistar rats (age 10–12 weeks; body weight 175 ± 10 g) were divided into four groups, namely control group, low-dose (LD) group, mid-dose (MD) group, high-dose (HD) group, and received GO at the doses of 0.0 (vehicle only, i.e., 0.1% Tween 80 in autoclaved normal saline), 0.4, 2.0, and 10.0 mg/kg body weight respectively ($N =$ 6 for each group). The LD_{50} determination for carbon-based nanomaterials is not recommended due to their overall less toxicity and the high cost of nanomaterials. Therefore, the low dose (0.4 mg/kg) was selected on the basis of literature study as well as insights from our previous experiments with multiwalled carbon nanotubes (Awasthi et al. 2013). Mid- and high doses were determined by multiplying the minimum dose with a common factor of 5.

Table 1   Specifications of GO used in the study (reproduced from Nirmal et al. 2017b)

Parameter	Attributes
Physical form	Grey – Black, Fluffy, Very Light Powder
Preparation method	Modified Hummer's method
Suspension in water	
TEM image	
SEM image	
Thickness	0.8-2 nm
Lateral dimension	5-10 μm
Surface area (BET)	>350 m^2/g
Bulk density	0.121g/cc
Average numbers of layers	3-6
Elemental composition	C (%) 77.5, O (%) 16.0, S (%) 0.4, H (%) 1.2, N (%) 4.9

A homogenous suspension of various doses of GO was prepared in autoclaved normal saline with 0.1% Tween 80 by ultrasonication (Labman-probe sonicator, PRO-250) prior to animal administration. Tween 80 is a detergent and functions as surfactant. It aids in forming more stable and uniform water dispersion of GO. GO was injected intraperitoneally on alternate days for 30 days. The animals were housed at 25 ± 2 °C temperature (relative humidity 33–40%) and 12-h light dark cycle. Water and standard laboratory rat diet were provided ad libitum (Ashirwad Pvt. Ltd., Chandigarh, India). Animals were euthanized by cervical dislocation following the day of last treatment. Blood and organ samples were obtained and stored properly. Serum was acquired from the blood and used for the estimation of liver function enzymes. Liver lobes were fixed in Bouin's solution for histopathological examination. A part of the organ was stored at − 80 °C for biochemical estimations. The study was approved by the Institutional Animal Ethical Committee (approval no. 1678/GO/a/12CPCSEA).

Liver function tests

Liver function tests, namely, aspartate aminotransferase (AST/GOT), alanine transaminase (ALT/GPT), and alkaline phosphatase (ALP), were measured using commercial kits (Accuzyme GOT, Accuzyme GPT, and Accuzyme ALP respectively) from Accurex Biomedical Pvt. Ltd. (Mumbai) according to the manufacturer's protocol. Freshly isolated serum was mixed with working solution and the conversion of NADH to NAD was measured spectrophotometrically at 340 nm. Unit of enzyme activity was reported as IU/l.

Hemocompatibility

Blood was collected by intra-cardiac puncture and was stored immediately in fresh EDTA-coated vials at 4 °C. Hematological analysis was carried out by automated blood analyzer (Accurex; CBC 360 Plus). Blood parameters analyzed in the study included red blood cells (RBC), white blood cells (WBC), mean corpuscular hemoglobin (MCH), mean corpuscular hemoglobin concentration (MCHC), mean corpuscular volume (MCV), hemoglobin (Hb), platelets, and hematocrit (HCT).

Preparation of crude homogenate and mitochondrial fraction

Liver was homogenized in cold phosphate-buffered saline (50 mM, pH 7.4) containing 0.25 M sucrose (20% w/v homogenate). Homogenate was filtered through a four-layered cheesecloth. The filtrate (crude homogenate) was further processed to obtain mitochondrial fraction. The crude homogenate was centrifuged at $600g$ for 10 min at 4 °C. The supernatant was then centrifuged at $10,000g$ for 5 min at 4 °C. Resulting pellet was washed thrice with ice cold PBS and resuspended in buffered saline (Nirmal et al. 2017b).

Catalase

Catalase (CAT) activity was quantified according to the protocol of Aebi (1984). Briefly, 0.1 ml of mitochondrial fraction (containing 0.4–0.5 mg protein) was mixed with 2.9 ml of 50 mM PBS (pH 7.0) containing 12 mM H_2O_2. Absorbance was recorded spectrophotometrically at 240 nm immediately at an interval of 15 s for 2 min. The unit of enzyme activity was μmol of H_2O_2 decomposed/min/mg protein.

Malondialdehyde

TBARS assay was performed in crude homogenates for determination of malondialdehyde (MDA) concentration (Ohkawa et al. 1979). A reaction mixture was obtained by adding 1.0 ml 0.15 M Tris-HCl buffer (pH 7.4), 0.3 ml of 10 mM KH_2PO_4, 0.2 ml sample (crude homogenate containing 1–1.5 mg of protein), and 0.5 ml DW. One milliliter 10% TCA was added after incubation at 37 °C for 20 min with constant shaking followed by adding of 1.5 ml 1% TBA. The mixture was then heated in a boiling water bath for 60 min. Test tubes were incubated at 4 °C for 60 min. The mixture was extracted with a mixture of n-butanol and pyridine (15:1 v/v). Absorbance was measured spectrophotometrically at 532 nm. The amount of MDA was calculated using extinction coefficient $1.56 \times 10^6 \, M^{-1} \, cm^{-1}$. The concentration of MDA was expressed as nmol MDA/mg protein.

Histology of liver and kidney

Organs were fixed with Bouin's solution for 24 h followed by washing in running water and dehydrated in graded alcohol series. The organs were embedded in paraffin wax. Sections of 4–5 μm were obtained by a microtome and stained with hematoxylin and eosin. Slides were examined with a light microscope (DM 1000, Leica Microsystems, Germany) and photographed by attached digital camera (DFC 450C).

Histomorphometry

Histomorphometry was performed by ImageJ® (ImageJ, US National Institutes of Health, Bethesda, USA) on liver transverse sections stained with hematoxylin and eosin for all the groups (see ESM_3 in Online Resource). Hepatocytes with clear nuclei and boundaries were selected for analysis. For hepatocyte area (HA), hepatocyte perimeter (HP), nuclei area (NA), and nuclei perimeter (NP), on average, 50 hepatocytes were selected randomly from each animal totaling 300 observations per group. Selected hepatocytes were also used for

nuclei parameters as well. Chosen hepatocytes and nuclei were outlined by free hand drawing tool for area and perimeter measurements. For sinusoidal area measurements, 10 randomly selected transverse sections were analyzed per animal, totaling 60 measurements per group by the free drawing selection method. Sinusoidal area was also measured in the selected sections by the thresholding method in the software. Hepatocyte and section selections for analysis were done by an experienced judge who was blinded for various treatment groups. For scoring, pathological changes in liver tissue, 10 randomly selected transverse sections were observed carefully for pathological signs in each animal. Pathological signs in liver that were checked included instances of vacuolations, inflammatory areas, necrotic areas, pyknotic nuclei, deformed cells, and dilated sinusoids. Presence of each pathological sign was given 1 score while absence was given 0 score. Similar process was employed for kidney pathology score. Pathologies for kidney that were scored were the following: inflammatory areas, abnormal glomeruli, dilated tubules, and necrotic spots.

Statistical analysis

All values were reported as mean ± standard deviation (SD). Statistical significance was tested using the GraphPad Prism (version 8.0.2) software. One-way ANOVA was performed followed by Tukey's honest significant difference (HSD) test for multiple comparisons. $p \leq 0.05$ was considered significant.

Results

General health

Intraperitoneal administration of GO did not elicit noticeable change in behavior. Animals exhibited aggressiveness, piling, lethargy, and change in gait in treated as well as control group.

Other behaviors such as thirst, salivation, food avoidance, and shivering were not observed (data provided in Online Resource, ESM_1). Liver and kidney indices did not differ significantly in treated animals as compared with the control (Table 2). Visible inspection of liver clearly showed progressive darkening of liver tissue in the case of treated rats (Fig. 1).

Biochemical parameters

Serum levels of ALT, AST, and ALP were increased significantly in high-dose treated animals compared with the control animals as shown in Table 2. Activities of these enzymes were insignificantly different from control ($p \leq 0.05$) in low- and mid-dose groups. CAT activity in liver tissue homogenates was diminished in the case of HD group. CAT activity in control group was 28.35, whereas in LD, MD, and HD groups, it was found to be 28.99, 26.99, and 20.31 μmol of H_2O_2 decomposed/min/mg protein, respectively. However, changes in the case of LD and MD group were not significant. MDA levels were elevated in rats exposed to mid- and high doses of GO in comparison with the control as given in Table 2.

Hemocompatibility

Hematology analysis demonstrated no major clinical signs in treated rats as compared with the control. However, hematocrit value increased (45.39%) in high-dose treated rats than that of control (39.16%). Effects on other blood parameters were not statistically significant ($p \leq 0.05$) (Table 3).

Histopathological and histomorphometric observations

The control group exhibited regular lobular arrangement with intact hepatocytes and sinusoids. The low-dose group also showed similar features with rare instances of vacuolations and occasional hepatocytic damage (Fig. 2a, b). Pathological

Table 2 Organ indices, activities of ALT, AST, ALP, and CAT, and concentration of MDA in control and GO-treated animals

Parameters	Control (0.0 mg/kg)	Low dose (0.4 mg/kg)	Mid-dose (2.0 mg/kg)	High dose (10.0 mg/kg)
Liver index	0.029 ± 0.002	0.027 ± 0.003	0.026 ± 0.003	0.029 ± 0.002
Kidney index	0.0043 ± 0.0002	0.0042 ± 0.0003	0.0045 ± 0.0004	0.0043 ± 0.0003
AST (IU/l)	219.50 ± 15.45	233.00 ± 21.15	239.30 ± 19.80	293.40* ± 12.03
ALT (IU/l)	56.67 ± 7.55	56.83 ± 9.89	62.17 ± 9.00	82.50* ± 10.77
ALP (IU/l)	230.50 ± 16.07	239.70 ± 18.64	246.70 ± 19.97	290.00* ± 8.92
CAT (μmol of H_2O_2 decomposed/min/mg protein)	28.35 ± 2.67	28.99 ± 1.69	26.99 ± 3.63	20.31* ± 2.84
MDA (nmol MDA/mg protein)	7.60 ± 0.56	7.69 ± 0.96	8.86* ± 0.48	9.82* ± 0.74

Each value is represented as mean ± standard deviation for each treatment group ($n = 6$). Value(s) with asterisk (*) show(s) statistically significant difference as compared with control within the same row, $p \leq 0.05$

AST, aspartate aminotransferase; *ALT*, alanine transaminase; *ALP*, alkaline phosphatase; *CAT*, catalase; *MDA*, malondialdehyde

Fig. 1 Representative photographs of liver from control, LD, MD, and HD groups. **a** Control. **b** LD group. **c** MD group. **d** HD group. Liver from the HD group shows visible darkening and entangled agglomerates of GO (arrowheads)
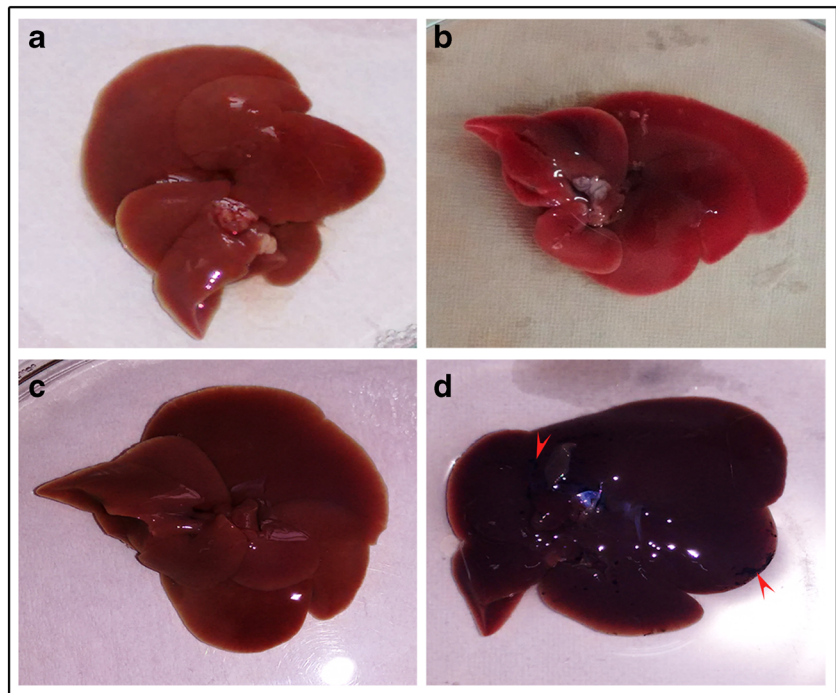
features were very pronounced in mid- and high-dose groups. Pathology score showed statistically significant number of anomalies in these groups as compared with the control and low-dose groups. As shown in Fig. 2c–k, mild inflammation around central and portal veins, exudate, vacuolations, hepatocyte shape changes, and pyknotic nuclei were observed mostly in mid- and high-dose treated groups. Hepatocytic injury and anomalies were supported by the histomorphometric observations carried out in all the groups (Table 4). The mean HA was 280.2 ± 46.24 μm^2 in control while in LD, MD, and HD, it was found to be 281.7 ± 59.10, 261.6 ± 47.57, and 267.6 ± 61.14 μm^2, respectively. The decrease in mid- and high-dose group was statistically significant. The mean HP

was also lowered in both MD and HD groups compared with control; however, only the MD group showed statistical significance as shown in Table 4. The mean NA also exhibited general decrease in treated groups with a statistically significant reduction in the mid-dose group only as compared with the control. NP mean values did not differ significantly among the control and treated animals. Sinusoidal area measurements by both the methods showed a significant increase in sinusoidal area in the high-dose treated group (11.13 ± 6.25 by SAT and 6.48 ± 3.00 by SAS) in comparison with that of control (5.45 ± 2.15 by SAT and 5.19 ± 1.77 by SAS). Kidney pathology revealed mild damage in treatment groups. Pathological features like distorted glomeruli, tubular dilations, and

Table 3 Effects of graphene oxide exposure on different parameters of blood in Wistar rats at different dose levels

Parameters	Control (0.0 mg/kg)	Low dose (0.4 mg/kg)	Mid-dose (2.0 mg/kg)	High dose (10.0 mg/kg)
RBC ($\times 10^{12}$/l)	7.61 ± 0.39	7.39 ± 0.64	7.53 ± 1.03	6.64 ± 1.59
WBC ($\times 10^9$/l)	6.00 ± 0.66	5.94 ± 0.44	7.13 ± 0.80	6.03 ± 1.21
Hematocrit (%)	39.16 ± 3.56	40.44 ± 2.81	42.71 ± 3.57	$45.39^* \pm 3.86$
MCH (pg)	16.13 ± 0.75	15.88 ± 0.89	16.23 ± 0.95	16.65 ± 1.77
MCHC (g/dl)	33.15 ± 2.46	32.97 ± 1.57	33.10 ± 2.70	33.97 ± 1.87
MCV (fl)	50.03 ± 2.41	49.12 ± 2.77	50.66 ± 4.95	47.79 ± 3.67
Platelets ($\times 10^9$/l)	351.50 ± 122.90	307.20 ± 104.00	314.20 ± 68.24	331.30 ± 107.20
Hb (g/dl)	12.18 ± 0.68	11.68 ± 1.09	11.72 ± 1.17	11.10 ± 1.22

Each value is represented as mean ± standard deviation for each treatment group ($n = 6$). Value(s) with asterisk (*) show(s) statistically significant difference as compared with control within the same row, $p \le 0.05$

RBC, red blood cells; *WBC*, white blood cells; *MCH*, mean corpuscular hemoglobin; *MCHC*, mean corpuscular hemoglobin concentration; *MCV*, mean corpuscular volume; *Hb*, hemoglobin

Fig. 2 Hepatic histological features observed in control and GO-treated Wistar rats. **a** Normal arrangement of hepatocytes at lower magnification (scale bar, 50 μm). **b** Normal arrangement of hepatocytes at higher magnification (scale bar, 25 μm). **c** Liver T.S. showing damaged portal vein (PV; circle), dilated sinusoid (arrow), and exudate filled vacuoles (arrow head). Scale bar is 50 μm. **d** Inflammatory cell filtration through portal vein (PV, arrow); BD, biliary duct; HA, hepatic artery (scale bar 50 μm). **e** Inflammatory cells crossing portal vein at higher magnification (arrow). Scale bar 15 μm. **f** T.S. showing edema-filled space (scale bar 50 μm). **g** and **h** show the presence of multiple vacuolations small (small arrow) and large (big arrow) and edema-filled space (arrowhead). Scale bar 25 μm. **i** Hepatocytes with elongated shape and displaced nuclei (arrow); scale bar 15 μm. **j** Hepatocytes with pyknotic nuclei (arrowhead); scale bar 15 μm. **k** Pathology score in liver histological sections in control and GO-treated rats. Asterisks (*) show statistically significant difference compared with the control, $p \leq 0.05$
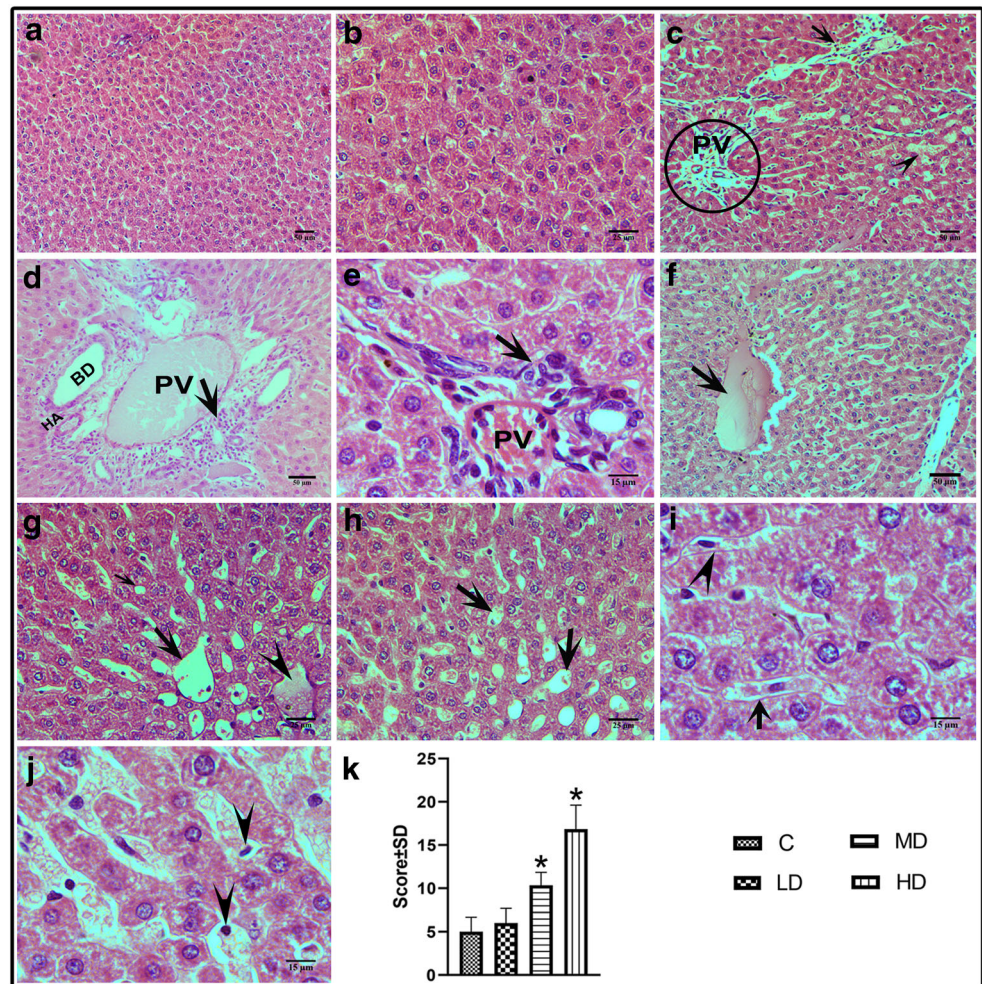
inflammation were observed in treated groups although the scores did not show statistical significance except in the high-dose group (Fig. 3a–e).

Discussion

Carbon nanomaterials (CNMs) are relatively less toxic than the metal-based nanomaterials. However, CNMs owing to their variety of shapes, like needle-shaped carbon nanotubes, amorphous carbon black, and sheet-shaped graphene family nanomaterials, generate different toxic responses in living systems. In the current study, we have evaluated the toxic effects of sheet-shaped graphene oxide with thickness of 0.8–2 nm and average lateral size of 5–10 μm. Liver is the primary organ where nanoparticles accumulate and generate toxic effects (Almeida et al. 2011). Intraperitoneally administered particles make entry into liver tissue through hepatic portal vein. Biodistribution studies have shown that GO with lateral sizes ranging from 8 to 800 nm accumulates mostly in lungs and liver of treated rats (Zhang et al. 2011; Kurantowicz et al.

2015). Therefore, the present study examined effects of GO on liver of adult Wistar rats.

In the present study, general health indicators were similar to that of control which indicates that GO does not produce any drastic toxicity to general body metabolism. These findings are in line with an in vivo work done by Kim et al. (2018). The study observed that short-term inhalation exposure to GO (thickness ~ 1 nm and lateral size 0.5 to 5 μm) at high concentration (9.78 ± 0.29 mg/m³) does not cause any major body weight and organ weight changes in male Sprague-Dawley rats. However, in a study by Amrollahi-Sharifabadi et al. (2018), intraperitoneal exposure led to changes in body weight gain in animals after 21 days which were treated with 500 mg/kg, but not in the animals exposed to 150 or 50 mg/kg dose of GO nanoplatelets having 0.8–2 nm thickness and 5–10 μm diameter. As the physical dimensions of GO are comparable in studies mentioned above, the difference in results may be attributed to the magnitude and route of dose administered.

It is well established that increased levels of ALT, AST, and ALP are associated with inflammation and injury to the hepatic tissue (Kew 2000; Giannini et al. 2005; Gowda et al. 2009). In the current study, all three enzymes were found to be

Table 4 Morphometric measurements in histological sections of liver tissues of control and GO-treated Wistar rats

| Parameters	Control (0.0 mg/kg)	Low dose (0.4 mg/kg)	Mid-dose (2.0 mg/kg)	High dose (10.0 mg/kg)
Hepatocyte area (HA; μm^2)	280.2 ± 46.24	281.7 ± 59.10	$261.6^* \pm 47.57$	$267.6^* \pm 61.14$
Hepatocyte perimeter (HP; μm)	63.83 ± 12.47	63.14 ± 11.53	$60.69^* \pm 12.61$	61.74 ± 13.53
Nuclei Area (NA; μm^2)	48.30 ± 5.31	47.89 ± 5.80	$46.72^* \pm 6.34$	47.04 ± 8.53
Nuclei Perimeter (NP; μm)	25.10 ± 2.69	24.98 ± 2.50	24.80 ± 2.75	24.65 ± 3.01
Sinusoidal Area by Thresholding Method (SAT; %)	5.45 ± 2.15	6.60 ± 2.39	6.80 ± 3.32	$11.13^* \pm 6.25$
Sinusoidal Area by Selection Method (SAS; %)	5.19 ± 1.77	5.67 ± 1.96	5.82 ± 2.31	$6.48^* \pm 3.00$
Liver Pathology Score (LPS)	5.00 ± 1.67	6.00 ± 1.67	$10.33^* \pm 1.51$	$16.83^* \pm 2.79$
Kidney Pathology Score (KPS)	0.83 ± 0.75	1.33 ± 1.03	2.33 ± 1.75	$4.00^* \pm 2.61$

Each value represents mean ± standard deviation for each treatment group. Value(s) with asterisk (*) show(s) statistically significant difference as compared with control within the same row

$^*p \leq 0.05$

elevated as compared with control at a dose of 10.0 mg/kg, although the changes were insignificant at lower doses. Our results are in agreement with the study by Patlolla et al. (2017). Repeated exposure to GO (spherical shaped sheets with average diameter of 40 nm) at 20 and 40 mg/kg for 5 days

resulted into elevation of serum levels of ALT and ALP. Similarly, Li et al. (2016) injected GO having lateral size 100–500 nm via tail veins of the Sprague-Dawley rats in three increasing doses for 7 days. Results clearly demonstrated inflammatory damage to lung, liver, and spleen at the highest

Fig. 3 Representative microphotographs of H-E stained sections of kidney from control and GO-treated Wistar rats. **a** Compact glomeruli and renal tubules in the control group. **b** Low-dose treated tissue shows normal glomeruli and kidney tubules. **c** Kidney T.S. showing damaged kidney tubules (arrow) and normal glomeruli in the tissue of mid-dose treated rat. **d** High-dose treated section showing abnormal glomerulus (arrow) and edema-filled space (arrowhead). **e** Pathology score in kidney histological sections measured in control and GO-treated rats. Scale bar is 50 μm. Asterisks (*) show statistically significant difference as compared with control, $p \leq 0.05$
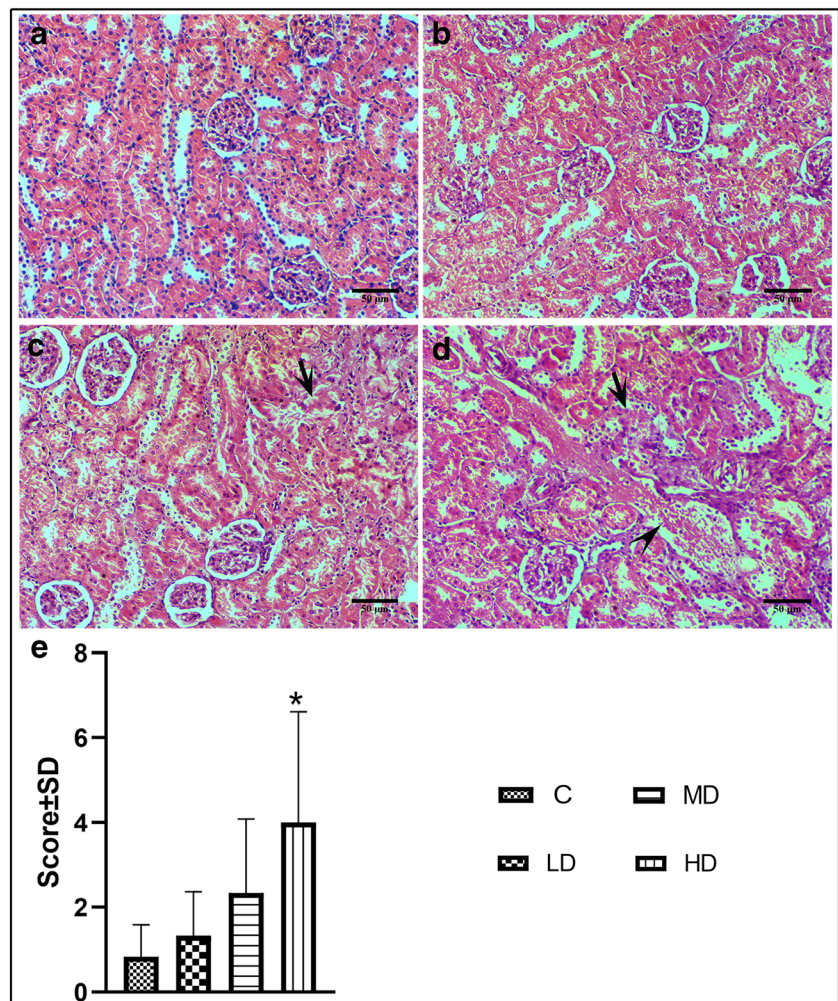
dose (10 mg/kg). At a similar dose and route of administration with greater lateral size (10–800 nm), GO induced significant toxic effects in lungs, including inflammation cell infiltration, pulmonary edema, and granuloma formation in mice (Zhang et al. 2011). There are few contrasting reports which found negligible effects due to GO exposure. For instance, Kim et al. (2018) studied the effects after inhalation exposure in male Sprague-Dawley rats. They did not observe any significant elevation in bronchoalveolar lavage fluid inflammatory markers. The above reports indicate that graphene oxide is capable of inducing inflammation in the hepatic tissue especially at higher doses. Several in vitro reports have shown that GO (with lateral sizes from 200 to 700 nm) damages the cell membranes and enter cytosol (Lammel et al. 2013; Duan et al. 2017). Therefore, it is proposed that GO entered liver parenchyma and damaged cells in liver tissue especially at the entry point like hepatic veins. This is supported by histological analysis in our study which shows inflammatory cells crossing the portal vein boundary (Fig. 2 d and e). Reports also suggest that GO with larger lateral sizes (from 750 to 1300 nm) leads to greater degree of inflammation due to high adsorption of cells and less phagocytosis (Ma et al. 2015).

To understand the mechanism of toxicity, we examined the antioxidant defense of liver tissue as this is a major pathway through which CNMs inflict damage upon living cells (Bai et al. 2010; Patlolla et al. 2011; Nirmal et al. 2017a, b). GO-mediated damage to cellular membranes and organelles may lead to higher level of ROS which is responsible for higher lipid peroxidation (Jarosz et al. 2016; Gurunathan et al. 2019). In an interesting work by Mittal et al. (2016), graphene oxide derivatives successfully internalized in human lung cells and induced oxidative stress. The researchers used three kinds of GO derivatives, viz. graphene oxide with 0.2 μm to 0.6 μm, thermally reduced GO (TRGO) having smaller flake sizes ranging from 50 to 250 nm, and chemically reduced GO (CRGO) with 100 nm to 400 nm lateral size. The oxidative stress induction was found to be more with reduced lateral size and increased functional groups. The present study reports that GO at higher doses (10 mg/kg) is capable of impacting antioxidant enzymes and generating ROS as evident by enhanced MDA level in liver tissue. Our report is also consistent with the findings of Patlolla et al. (2017). The group found significant elevation in ROS and lipid peroxidation at higher doses of GO (20 and 40 mg/kg) following five repeated exposures for 5 days. Therefore, oxidative damage appears to be a valid mechanism for toxicity of GO to the hepatic tissue.

The biochemical findings discussed above were supported by histopathological and histomorphometric analyses. The current study observed inflammatory areas around the central vein and portal veins. Vacuolations and hepatocytic injury are evident in Fig. 2. The mean HA was significantly decreased in the mid- and high-dose group. This is a sign of shrinkage in hepatocytes. This may be a result of loss of cytoplasm or necrotic cell death. It is important to note that in HD tissues, enlargement of hepatocytes was also observed as indicated by greater standard deviation. Similar observations were made with hepatocyte perimeter and nuclei area measurements. Reduction in NA supports the presence of pyknotic nuclei as seen in histopathology. Sinusoidal area measurements revealed larger sinusoidal spaces which correlates with the increased presence of vacuolations and dilated sinusoids especially in MD and HD groups (Table 4). Mild nephrotoxicity was also found through histological inspection. Toxicity observed in kidney suggests that the GO nanosheets may accumulate in this organ and generate toxicity. Li et al. (2016) observed that intravenous injections for 7 days with 2.5, 5, or 10 mg/kg dose of GO (lateral size 10–800 nm) caused inflammation in the liver, lung, and spleen. The capillaries became hyperemic and enlargement of hepatic sinusoids and central veins was observed. Similarly, Patlolla et al. (2017) demonstrated morphological changes in liver tissue such as cell disruption, vacuolations, central vein injury, and liver atrophy post exposure to 20 and 40 mg/kg in a dose-dependent fashion. However, in the report by Kim et al. (2018), graphene oxide (9.78 ± 0.29 mg/m^3) did not produce any significant histopathological injury in liver and kidneys of rats after inhalation exposure for 6 h/day for 5 days. The differences in toxicity outcomes may be related to the route of administration. It is also noteworthy that GO average lateral size in the former study was 40 nm while in the latter ranged from 0.5 to 5 μm. Physico-chemical characteristics play an important role in toxicity outcomes resulting from exposure to GO. Variations in results due to these factors pose a formidable challenge in toxicity assessments. Carefully controlled studies taking physico-chemical characteristics into consideration are needed to explore the various aspects of in vivo toxicity generated by GO exposure.

Limitations of study

Biodistribution study could have demonstrated the distribution of GO into various organs of the body. The current study could not show the intracellular localization of GO sheets in the absence of examination of hepatic tissue by TEM. More parameters, including inflammatory markers, immunohistochemistry, and special staining methods, could have revealed more toxicity aspects and could have supported the observation of our study. These parameters could not be performed due to the lack of funds. Greater lateral size of GO limited the power of study due to less penetration of larger GO sheets into the deeper parenchyma of liver. The dose levels in the present study do not represent the real-life exposure scenario due to high dose amounts and selected route. Nevertheless, sub-acute studies are a quick way to demonstrate potential toxic effects of various toxicants. Smaller exposure doses for longer duration through oral route would have been more relevant scenario.

Conclusion

The current study examined the toxicity following a sub-acute exposure of GO in Wistar rats. Results of the study indicated a dose-dependent toxicity. Serum levels of liver function enzymes were found to be elevated implying inflammation and injury to the liver. Histopathological lesions in hepatic tissue supported the biochemical observations. The toxicity generation seems to be a result of elevated oxidative stress as evident by MDA and CAT levels. These findings are clearly showing that GO with larger lateral sizes possesses considerable toxic potential to mammalian liver and thorough toxicity studies are needed before these nanosheets are used for biomedical purposes.

Compliance with ethical standards

Conflict of interest The authors declare that they have no conflict of interest.

References

Aebi H (1984) Catalase in vitro. Methods Enzymol 105:121–126

Almeida JPM, Chen AL, Foster A, Drezek R (2011) In vivo biodistribution of nanoparticles. Nanomedicine 6(5):815–835

Amrollahi-Sharifabadi M, Koohi MK, Hablolvarid MH, Hassan J, Seifalian AM (2018) In vivo toxicological evaluation of graphene oxide nanoplatelets for clinical application. Int J Nanomedicine 13:4757–4769

Awasthi KK, John PJ, Awasthi A, Awasthi K (2013) Multi walled carbon nanotubes induced hepatotoxicity in Swiss albino mice. Micron 44:359–364

Bai Y, Zhang Y, Zhang J, Mu Q, Zhang W, Butch ER, Snyder SE, Yan B (2010) Repeated carbon nanotube administrations in male mice cause reversible testis damage without affecting fertility. Nat Nanotechnol 5:683–689

Beitollahi H, Safaei M, Tajik S (2019) Application of graphene and graphene oxide for modification of electrochemical sensors and biosensors: a review. Int J Nano Dimens 10(2):125–140

Coros M, Pogacean F, Magerusan L, Socaci C, Pruneanu S (2019) A brief overview on synthesis and applications of graphene and graphene-based nanomaterials. Front Mater Sci 13(1):23–32

Das T, Sharma BK, Katiyar AK, Ahn JH (2018) Graphene-based flexible and wearable electronics. J Semicond 39:011007

Dreyer DR, Park S, Bielawski CW, Ruoff RS (2010) The chemistry of graphene oxide. Chem Soc Rev 39:228–240

Duan G, Zhang Y, Luan B, Weber JK, Zhou RW, Yang Z, Zhao L, Xu J, Luo J, Zhou R (2017) Graphene-induced pore formation on cell membranes. Sci Rep 7:42767

Giannini EG, Testa R, Savarino V (2005) Liver enzyme alteration: a guide for clinicians. CMAJ 172(3):367–379

Gowda S, Desai PB, Hull VV, Math AA, Vernekar SN, Kulkarni SS (2009) A review on laboratory liver function tests. Pan Afr Med J 3:17

Gurunathan S, Arsalan Iqbal M, Qasim M, Park CH, Yoo H, Hwang JH, Uhm SJ, Song H, Park C, Do JT, Choi Y, Kim JH, Hong K (2019)

Evaluation of graphene oxide induced cellular toxicity and transcriptome analysis in human embryonic kidney cells. Nanomaterials (Basel) 9(7):969

Jarosz A, Skoda M, Dudek I, Szukiewicz D (2016) Oxidative stress and mitochondrial activation as the main mechanisms underlying graphene toxicity against human cancer cells. Oxidative Med Cell Longev 10:1155

Kew MC (2000) Serum aminotransferase concentration as evidence of hepatocellular damage. Lancet 355:591–592

Khan M, Tahir MN, Adil SF, Khan HU, Siddiqui MR, Al-warthan AA, Tremel W (2015) Graphene based metal and metal oxide nanocomposites: synthesis, properties and their applications. J Mater Chem A 3:18753–18808

Kim YH, Jo MS, Kim JK, Shin JH, Baek JE, Park HS (2018) Short-term inhalation study of graphene oxide nanoplates. Nanotoxicology 12(3):224–238

Kurantowicz N, Strojny B, Sawosz E, Jaworski S, Kutwin M, Grodzik M, Wierzbicki M, Lipińska L, Mitura K, Chwalibog A (2015) Biodistribution of a high dose of diamond, graphite, and graphene oxide nanoparticles after multiple intraperitoneal injections in rats. Nanoscale Res Lett 10(1):398

Lammel T, Boisseaux P, Fernandez-Cruz ML, Navas JM (2013) Internalization and cytotoxicity of graphene oxide and carboxyl graphene nanoplatelets in the human hepatocellular carcinoma cell line Hep G2. Part Fibre Toxicol 10:27

Li B, Yang J, Huang Q, Zhang Y, Peng C, Zhang Y, He Y, Shi J, Li W, Hu J, Fan C (2013) Biodistribution and pulmonary toxicity of intratracheally instilled graphene oxide in mice. NPG Asia Mater 5:e44. https://doi.org/10.1038/am.2013.7

Li Y, Wang Y, Tu L, Chen D (2016) Sub-acute toxicity study of graphene oxide in the Sprague-Dawley rat. Int J Environ Res Public Health 13(11):1149

Lonkar SP, Abdala AA (2014) Applications of graphene in catalysis. J Thermodyn Catal 5(2):132–137

Ma J, Liu R, Wang X, Liu Q, Chen Y, Valle RP, Zuo YY, Xia T, Liu S (2015) Crucial role of lateral size for graphene oxide in activating macrophages and stimulating pro-inflammatory responses in cells and animals. ACS Nano 9(10):10498–10515

Mendonça MCP, Soares ES, Bispo de Jesus M et al (2016) Reduced graphene oxide: nanotoxicological profile in rats. J Nanobiotechnol 14(1):53

Mittal S, Kumar V, Dhiman N, Chauhan LKS, Pasricha R, Pandey AK (2016) Physico-chemical properties based differential toxicity of graphene oxide/reduced graphene oxide in human lung cells mediated through oxidative stress. Sci Rep 6:39548

Mohan VB, Lau KT, Hui D, Bhattacharyya D (2018) Graphene-based materials and their composites: a review on production, applications and product limitations. Compos Part B: Eng 142:200–220

Nirmal NK, Awasthi KK, John PJ (2017a) Effects of hydroxyl-functionalized multi-walled carbon nanotubes on sperm health and testes of Wistar rats. Toxicol Ind Health 33(6):519–529

Nirmal NK, Awasthi KK, John PJ (2017b) Effects of nano-graphene oxide on testis, epididymis and fertility of Wistar rats. Basic Clin Pharmacol Toxicol 121(3):202–210

Ohkawa H, Ohishi N, Yagi K (1979) Assay for lipid peroxides in animal tissues by thiobarbituric acid reaction. Anal Biochem 95(2):351–358

Ou L, Song B, Liang H, Liu J, Feng X, Deng B, Sun T, Shao L (2016) Toxicity of graphene-family nanoparticles: a general review of the origins and mechanisms. Part Fibre Toxicol 13(1):57

Pang L, Dai C, Bi L, Guo Z, Fan J (2017) Biosafety and antibacterial ability of graphene and graphene oxide in vitro and in vivo. Nanoscale Res Lett 12(1):564

Patlolla AK, Berry A, Tchounwou PB (2011) Study of hepatotoxicity and oxidative stress in male Swiss-Webster mice exposed to

functionalized multi-walled carbon nanotubes. Mol Cell Biochem 358(1–2):189–199

Patlolla AK, Rondalph J, Tchounwou PB (2017) Biochemical and histopathological evaluation of graphene oxide in Sprague-Dawley rats. Austin J Environ Toxicol 3(1):1021

Phiri J, Gane P, Maloney TC (2017) General overview of graphene: production, properties and application in polymer composites. Mater Sci Eng B 215:9–28

Priyadarsini S, Mohanty S, Mukherjee S, Basu S, Mishra M (2018) Graphene and graphene oxide as nanomaterials for medicine and biology application. J Nanostruct Chem 8:123–137

Saha A, Basiruddin SK, Ray SK, Roy SS, Jana NR (2010) Functionalized graphene and graphene oxide solution via polyacrylate coating. Nanoscale 2:2777–2782

Shen H, Zhang L, Liu M, Zhang Z (2012) Biomedical applications of graphene. Theranostics 2(3):283–294

Singh R, Tripathi C (2018) Electrochemical exfoliation of graphite into graphene for flexible supercapacitor application. Mater Today-Proc 5(1):1125–1130

Wang K, Ruan J, Song H, Zhang J, Wo Y, Guo S, Cui D (2011) Biocompatibility of graphene oxide. Nanoscale Res Lett 6(1):8

Wang Z, Ciacchi LC, Wei G (2017) Recent advances in the synthesis of graphene-based nanomaterials for controlled drug delivery. Appl Sci 7(11):1175–1193

Yang J, Hu PA, Yu G (2019) Perspective of graphene-based electronic devices: graphene synthesis and diverse applications. APL Mater 7(2):020901–020907

Zhang X, Yin J, Peng C, Hu W, Zhu Z, Li W, Fan C, Huang Q (2011) Distribution and biocompatibility studies of graphene oxide in mice after intravenous administration. Carbon 49(3):986–995